AIMS Mathematics, 10(3): 5124–5142.
DOI: 10.3934/math.2025235
Received: 02 January 2025
Revised: 08 February 2025
Accepted: 27 February 2025
Published: 06 March 2025

https://www.aimspress.com/journal/Math

Research article

Exact and numerical solutions of the generalized breaking soliton system: Insights into non-linear wave dynamics

Amer Ahmed[1,2,*], **Abdulghani R. Alharbi**[2] **and Ishak Hashim**[1,3]

[1] Department of Mathematical Sciences, Faculty of Science & Technology, Universiti Kebangsaan Malaysia, 43600 UKM Bangi, Selangor, Malaysia

[2] Department of Mathematics, College of Science, Taibah University, 42353, Medina, Saudi Arabia

[3] Nonlinear Dynamics Research Center (NDRC), Ajman University, Ajman, P.O. Box 346, United Arab Emirates

* **Correspondence:** Email: amer.abdulfattah.ahmed@gmail.com; Tel: +601118927524.

Abstract: In this paper, we examined the (2+1)-dimensional generalized breaking soliton system (GBSS), an adaptable framework that accurately describes the three-dimensional, wave-dominated interactions occurring in many non-linear media, i.e., fluids, plasmas, and optical fibers. We used an improved F-expansion technique to generate new families of exact solitonic and periodic wave solutions, significantly enlarging the well-studied solution space and providing insight into the complicated interaction between multi-pulse solitons. Validation of these results and an assessment of their stability were carried out by developing a numerical scheme based on finite difference and undertaking a detailed error and stability analysis, demonstrating unconditional stability across a range of parameter values. The results provide new insights into the interplay of dispersion, non-linearity, and cross-wave coupling in governing soliton formation and energy transport in multidimensional systems. In addition to its theoretical importance, this work can provide valuable practical information on engineering applications such as soliton-based communications and wave control applications in fluid systems. This study offers a new methodology to investigate more complex non-linear wave phenomena by integrating the power of symbolic computation with that of robust numerical verification, opening new opportunities for further developments in soliton-driven technologies.

Keywords: non-linear wave dynamics; exact solutions; numerical solutions; modified F-expansion method; finite difference method; soliton performance; energy transportation; wave interactions
Mathematics Subject Classification: 35A24, 35B35, 35Q51, 35Q92, 65N06, 65N40, 65N45, 65N50

1. Introduction

The investigation of solitonic solutions for non-linear evolution equations (NLEEs) is essential to advancing several scientific and technological fields, including non-linear movement [1], ocean engineering [2], fibre optics [3, 4], high-frequency waves [5, 6], plasma physics [7], nanoscale components [8], and fluid interaction [9, 10]. Such singular wave phenomena, called solitons, maintain their shape and energy over large distances, which is crucial for understanding the activities of complex non-linear systems. Solitons are essential for the study of non-linear systems due to their durability and ability to capture essential knowledge on system behavior [11]. The designation and scrutiny of solitonic solutions not only enhance our abstract understanding but also encourage pragmatic improvements in innovations based on non-linear phenomena [12]. Beyond the span, absorbing phenomena such as rogue waves and transient and localized waves that appear unexpectedly and disperse without trace have been detected in deep probes in non-linear situations [13]. Rogue surges have been detected in a variety of contexts [14–17]. Given the significant importance of solitonic solutions in understanding and advanced non-linear frameworks throughout multiple objectives, considerable efforts have been made to develop robust approaches to their compilation and verification. Over the past few decades, scientists have developed various methods to study and construct solitonic solutions for NLEEs. These methods include adjusting and developing classical Bäcklund transformations [18], Darboux transformations [19], as well as the Breather limit approach [20], Hirota bilinear method [21], generalized exponential rational function method [22–25], exponential rational function approach, sinh cosh approach [26], direct algebraic approach [27–29], improved modified extended tanh function approach [30, 31], fundamental (G'/G)-expansion method [32], and many others.

The main objective of the present research is to examine the (2+1)-dimensional generalized breaking soliton system (GBSS). This system is a robust theoretical framework to model the dispersion, non-linearity, and cross-wave coupling in media such as shallow water waves, optical fibre systems and magnetized plasma. While earlier studies focused on particular cases of GBSS, such as [18,25,33–35], the present work aims to derive the equation in a more complete and generalized form. By broadening the scope, this study seeks to uncover dynamic behaviors and solutions that may have been indifferent in previous studies of particular cases. The generalized form then ideally offers a unified perspective, which allows one to appreciate different non-linear phenomena that the GBSS encompasses and understand them theoretically better. This work not only improves upon earlier approaches but also contributes to the growing body of literature on more compact and efficient ways of studying non-linear evolution equations. The foundation of this work is the GBSS, which is formally expressed by the following equations:

$$\begin{aligned} &\Psi_t + \alpha\Psi_{xxx} + \beta\Psi_{xxy} + \gamma\Psi\Psi_x + \delta\Psi\Phi_x + \lambda\Psi_x\Phi = 0, \\ &\Psi_y = \Phi_x, \end{aligned} \tag{1.1}$$

where the parameters $\alpha, \beta, \gamma, \delta$, and λ are real parameters, and the functions $\Psi = \Psi(x, y, t)$ and $\Phi = \Phi(x, y, t)$ describe the values propagated in the direction of the two structures, respectively. Ψ_t is what governs the way the wave changes with time. The third derivative with respect to x gives $\alpha\Psi_{xxx}$, which denotes x-axial dispersion. Dispersion is a process that spreads out the wave so that the steepening of the wave due to the non-linear processes is reduced. The mixed derivative $\beta\Psi_{xxy}$ describes the spread in

x and y directions. Therefore, it shows the complicated interaction of waves in both directions. A non-linear term $\gamma\Psi\Psi_x$ represents the self-interaction of the wave. It implies that it is increasingly becoming steeper as the wave gets fatter in amplitude. This explains why waves with higher amplitude would travel faster, and the wave would become steep. In addition, the terms $\delta\Psi\Phi_x$ and $\lambda\Psi_x\Phi$ are interactions in both directions of the two wave fields that integrate the motion of the waves with respect to both axes. They show how waves travelling along one direction affect the motions of the waves travelling along a perpendicular direction. The second equation on the system 1.1, $\Psi_y = \Phi_x$, relates the two wave fields Ψ and Φ, implying that if there is a wave propagating in the y direction, there must also be a wave propagating in the x direction.

In a fluid dynamic context, the GBSS pertains to the interaction of surface waves that ripple in the water's surface with internal waves that develop in the water below the surface as a result of mechanical force in strata of different densities. Surface waves, which are caused by wind and gravity, typically have a short period and propagate quickly, while internal waves have larger wavelengths, a slower speed, and larger amplitudes. The GBSS captures these interactions by balancing non-linear effects from wave steepening (terms at the $\gamma\Psi\Psi_x$ level) with dispersive effects that drive wave dispersion (the $\alpha\Psi_{xxx}$ term). The cross-interaction terms $\delta\Psi\Phi_x$ and $\lambda\Psi_x\Phi$ express the energy flow between surface and interior waves while in contact. The situation might include internal waves being magnified by surface waves leading to a similar soliton non-linear interaction where the wave structure changes due to this interaction, such as breaking or waterfalls [36]. In the context of non-linear optics as well, this (2+1)-dimensional GBSS describes the interaction of light pulses, or solitons, travelling along optical fibers, where the non-linear refractive index and dispersion are balanced so that solitons can be generated. When these light pulses propagate through the fibre, they experience the influence of a non-linear medium, which induces pulse steepening and the effect of dispersion, which leads to pulse broadening. The GBSS integrates such dynamics through concepts such as $\alpha\Psi_{xxx}$ for dispersion and $\gamma\Psi\Psi_x$, which represents non-linear effects. The cross-interaction terms $\delta\Psi\Phi_x$ and $\lambda\Psi_x\Phi$ represent the coupling between two light pulses, which can propagate in different polarization modes or neighboring fibers, allowing for energy transfer and complex interactions. One such interaction is the steepening or a breakup into sub-pulses (the breaking soliton phenomena) of one pulse. Such modeling is critical for optical communications: A profound understanding of soliton behavior and interaction can transfer data with better quality and over longer distances [37]. Similarly, other applications of GBSS include alfvén waves in magnetized plasma, earthquake dynamics and seismic waves, and the interaction of gravity waves.

In the sections that follow, we analyze the exact and numerical solutions of the system (1.1). In Section 2, we adopt the F-exponential method to obtain the exact solutions to (1.1), which demonstrates that the technique is effective for constructing the analytical solutions for the system. Section 3 deals with obtaining numerical solutions using the finite difference method that supplements the analytical methodology, which simulates the system's behavior under certain conditions.

2. Exact solutions of the GBSS

The development equation related to the physical fields $\Psi(x, y, t)$ and $\Phi(x, y, t)$ in the variables x, y, and t is expressed as follows:

$$P_1(\Psi, \Psi_t, \Psi_x, \Psi_{xxx}, \Psi_{xxy}, \Psi_y, \Phi, \Phi_x, \dots) = 0. \tag{2.1}$$

First, we derive the travelling-wave solutions of system (1.1), which are formulated as follows:

$$\begin{aligned} \Psi(x,y,t) &= \rho(\zeta), \qquad \zeta = kx + cy - wt, \\ \Phi(x,y,t) &= \varphi(\zeta), \end{aligned} \tag{2.2}$$

where k, c are arbitrary constants and w is the wave speed. Subsequently, the non-linear formation (2.1) is simplified to the following ordinary differential equation:

$$P_2(\rho, \rho_\zeta, \rho_{\zeta\zeta\zeta}, \varphi, \varphi_\zeta, \dots) = 0, \tag{2.3}$$

where P_2 is a polynomial in $\varphi(\zeta)$, $\rho(\zeta)$, and their total derivatives with respect to ζ.

In accordance with the modified F-expansion method, the solutions of (2.3) are given by the form

$$\rho(\zeta) = \sum_{k=0}^{N} \mu_k \Pi(\zeta)^k + \sum_{k=1}^{N} \sigma_k \Pi(\zeta)^{-k}, \tag{2.4}$$

that $\Pi(\zeta)$ is a solution of the following differential equation:

$$\Pi'(\zeta) = \nu_0 + \nu_1 \Pi(\zeta) + \nu_2 \Pi(\zeta)^2, \tag{2.5}$$

where ν_0, ν_1, ν_2 are specified in Table 1 [38], and μ_k, σ_k are to be identified after that.

Table 1. The relations among ν_0, ν_1, ν_2, and the function $\Pi(\zeta)$.

ν_0	ν_1	ν_2	$\Pi(\zeta)$
$\nu_0 = 0.0$,	$\nu_1 = 1.0$,	$\nu_2 = -1.0$,	$\Pi(\zeta) = 0.5 + 0.5\tanh(0.5\zeta)$.
$\nu_0 = 0.0$,	$\nu_1 = -1.0$,	$\nu_2 = 1.0$,	$\Pi(\zeta) = 0.5 - 0.5\coth(0.5\zeta)$.
$\nu_0 = 0.5$,	$\nu_1 = 0.0$,	$\nu_2 = -0.5$,	$\Pi(\zeta) = \coth(\zeta) \mp \mathrm{csch}(\zeta)$, $\tanh(\zeta) \mp i\,\mathrm{sech}(\zeta)$.
$\nu_0 = 1.0$,	$\nu_1 = 0.0$,	$\nu_2 = -1.0$,	$\Pi(\zeta) = \tanh(\zeta)$, $\coth(\zeta)$.
$\nu_0 = 0.5$,	$\nu_1 = 0.0$,	$\nu_2 = 0.5$,	$\Pi(\zeta) = \sec(\zeta) \pm \tan(\zeta)$, $\csc(\zeta) \mp \cot(\zeta)$.
$\nu_0 = \mp 1.0$,	$\nu_1 = 0.0$,	$\nu_2 = \mp 1.0$,	$\Pi(\zeta) = \tan(\zeta)$, $\cot(\zeta)$.
$\nu_0 = 0.0$,	$\nu_1 = 1.0$,	$\nu_2 \neq 0.0$,	$\Pi(\zeta) = 1/\left(\exp(-\zeta) - \nu_2\right)$.
ν_0 is arb. const.,	$\nu_1 \neq 0.0$,	$\nu_2 = 0.0$,	$\Pi(\zeta) = \left(\exp(\nu_1\,\zeta) - \nu_0\right)/\nu_1$.

The modified F-expansion method gives a successful approach to obtain solutions using the function $\Pi(\zeta)$. Transformations (2.2) will be used in (1.1) to simplify it into a system of ODEs given by

$$\begin{aligned} &-w\,\rho_\zeta + k^3\,\alpha\,\rho_{\zeta\zeta\zeta} + c\,k^2\beta\,\rho_{\zeta\zeta\zeta} + k\,\gamma\,\rho\rho_\zeta + k\,\delta\rho\varphi_\zeta + k\,\lambda\,\rho_\zeta\varphi = 0, \\ &c\,\rho_\zeta = k\,\varphi_\zeta. \end{aligned} \tag{2.6}$$

Integrating the second equation from the system (2.6), $c\,\rho_\zeta = k\,\varphi_\zeta$, with respect to ζ, gives us

$$\varphi = \frac{c}{k}\rho. \tag{2.7}$$

By substituting Eq (2.7) into the first equation of system (2.6) and performing one integration with regard to ζ, we obtain

$$k^2\,(k\,\alpha\, + c\,\beta)\,\rho_{\zeta\zeta} - w\,\rho + \frac{1}{2}\,(k\,\gamma\, + c\,\delta + c\,\lambda)\,\rho^2 = 0. \tag{2.8}$$

Balancing $\rho_{\zeta\zeta}$ with ρ^2 in Eq (2.8) gives the value of $N = 2$. According to the modified F-expansion method with $N = 2$, the general solutions of (2.8) are

$$\rho(\zeta) = \mu_0 + \mu_1\Pi(\zeta) + \mu_2\Pi(\zeta)^2 + \sigma_1\Pi(\zeta)^{-1} + \sigma_2\Pi(\zeta)^{-2}. \tag{2.9}$$

Here $\Pi(\zeta)$ is a solution of the following differential equation:

$$\Pi'(\zeta) = \nu_0 + \nu_1\Pi(\zeta) + \nu_2\Pi(\zeta)^2, \tag{2.10}$$

where ν_0, ν_1, ν_2 are specified in Table 1. To investigate the analytic solutions to (2.8), the following steps should be undertaken: First, substitute (2.9) and (2.10) into (2.8), group every coefficient of $\Pi(\zeta)^j$, $j = -4, ..., 4$, and set their values to zero. The result will give a system of equations for μ_0, μ_i, σ_i, $i = 1, 2$. Next, solve the resulting system using Wolfram Language. Finally, select the values of ν_0, ν_1, and ν_2, as well as the function $\Pi(\zeta)$ from Table 1, and replace these along with μ_0, μ_i, σ_i for $i = 1, 2$ into (2.9) to yield a collection of trigonometric functions and rational solutions to (2.8). With the methodology now established, we are able to proceed with adopting it. This enables us to reach the following conclusions:

Note that we will represent the mathematical statement $k(k\alpha + c\beta)$ with the symbol η for the reason of simplifying the notation in the solutions.

$$\begin{aligned}
\Psi_1 &= \frac{2^{2n-2}\,3\,k\eta}{c\,(\delta+\lambda)+\gamma k}\,\operatorname{sech}^2\left(2^{n-2}\left(k\,x + c\,y - 2^{2n-2}\,k\eta\,t\right)\right),\quad n\in\mathbb{R},\\
\Phi_1 &= \frac{2^{2n-2}\,3\,c\eta}{c\,(\delta+\lambda)+\gamma k}\,\operatorname{sech}^2\left(2^{n-2}\left(k\,x + c\,y - 2^{2n-2}\,k\eta\,t\right)\right),\quad n\in\mathbb{R}.
\end{aligned} \tag{2.11}$$

$$\begin{aligned}
\Psi_2 &= -\frac{2^{2n-2}\,3\,k\eta}{c\,(\delta+\lambda)+\gamma k}\,\operatorname{csch}^2\left(2^{n-2}\left(k\,x + c\,y - 2^{2n-2}\,k\eta\,t\right)\right),\quad n\in\mathbb{R},\\
\Phi_2 &= -\frac{2^{2n-2}\,3\,c\eta}{c\,(\delta+\lambda)+\gamma k}\,\operatorname{csch}^2\left(2^{n-2}\left(k\,x + c\,y - 2^{2n-2}\,k\eta\,t\right)\right),\quad n\in\mathbb{R}.
\end{aligned} \tag{2.12}$$

$$\begin{aligned}
\Psi_3 &= -\frac{2^{2n-2}\,k\eta}{c\,(\delta+\lambda)+\gamma k}\left(2 - 3\,\operatorname{sech}^2\left(2^{n-2}\left(kx + cy + 2^{2n-2}\,k\eta\,t\right)\right)\right),\quad n\in\mathbb{R},\\
\Phi_3 &= -\frac{2^{2n-2}\,c\eta}{c\,(\delta+\lambda)+\gamma k}\left(2 - 3\,\operatorname{sech}^2\left(2^{n-2}\left(kx + cy + 2^{2n-2}\,k\eta\,t\right)\right)\right),\quad n\in\mathbb{R}.
\end{aligned} \tag{2.13}$$

$$\begin{aligned}
\Psi_4 &= -\frac{2^{2n-2}\,k\eta}{c\,(\delta+\lambda)+\gamma k}\left(2 + 3\,\operatorname{csch}^2\left(2^{n-2}\left(kx + cy + 2^{2n-2}\,k\eta\,t\right)\right)\right),\quad n\in\mathbb{R},\\
\Phi_4 &= -\frac{2^{2n-2}\,c\eta}{c\,(\delta+\lambda)+\gamma k}\left(2 + 3\,\operatorname{csch}^2\left(2^{n-2}\left(kx + cy + 2^{2n-2}\,k\eta\,t\right)\right)\right),\quad n\in\mathbb{R}.
\end{aligned} \tag{2.14}$$

$$\Psi_{5,6} = -\frac{2\,k\eta}{c(\delta+\lambda)+\gamma k}\left(1 \mp \frac{3i}{\sinh\left(kx + cy + k\eta\,t\right) \pm i}\right),$$

$$\Phi_{5,6} = -\frac{2\,c\eta}{c(\delta+\lambda)+\gamma k}\left(1 \mp \frac{3i}{\sinh(kx+cy+k\eta\,t)\pm i}\right). \tag{2.15}$$

$$\begin{aligned}
\Psi_7 &= -\frac{2^{2n-2}\,3\,k\eta}{c\,(\delta+\lambda)+\gamma k}\sec^2\left(2^{n-2}\left(k\,x+c\,y+2^{2n-2}\,k\eta\,t\right)\right),\quad n\in\mathbb{R},\\
\Phi_7 &= -\frac{2^{2n-2}\,3\,c\eta}{c\,(\delta+\lambda)+\gamma k}\sec^2\left(2^{n-2}\left(k\,x+c\,y+2^{2n-2}\,k\eta\,t\right)\right),\quad n\in\mathbb{R}.
\end{aligned} \tag{2.16}$$

$$\begin{aligned}
\Psi_8 &= -\frac{2^{2n-2}\,3\,k\eta}{c\,(\delta+\lambda)+\gamma k}\csc^2\left(2^{n-2}\left(k\,x+c\,y+2^{2n-2}\,k\eta\,t\right)\right),\quad n\in\mathbb{R},\\
\Phi_8 &= -\frac{2^{2n-2}\,3\,c\eta}{c\,(\delta+\lambda)+\gamma k}\csc^2\left(2^{n-2}\left(k\,x+c\,y+2^{2n-2}\,k\eta\,t\right)\right),\quad n\in\mathbb{R}.
\end{aligned} \tag{2.17}$$

$$\begin{aligned}
\Psi_9 &= \frac{2^{2n-2}\,k\eta}{c\,(\delta+\lambda)+\gamma k}\left(2-3\sec^2\left(2^{n-2}\left(k\,x+c\,y-2^{2n-2}\,k\eta\,t\right)\right)\right),\quad n\in\mathbb{R},\\
\Phi_9 &= \frac{2^{2n-2}\,c\eta}{c\,(\delta+\lambda)+\gamma k}\left(2-3\sec^2\left(2^{n-2}\left(k\,x+c\,y-2^{2n-2}\,k\eta\,t\right)\right)\right),\quad n\in\mathbb{R}.
\end{aligned} \tag{2.18}$$

$$\begin{aligned}
\Psi_{10} &= \frac{2^{2n-2}\,k\eta}{c\,(\delta+\lambda)+\gamma k}\left(2-3\csc^2\left(2^{n-2}\left(k\,x+c\,y-2^{2n-2}\,k\eta\,t\right)\right)\right),\quad n\in\mathbb{R},\\
\Phi_{10} &= \frac{2^{2n-2}\,c\eta}{c\,(\delta+\lambda)+\gamma k}\left(2-3\csc^2\left(2^{n-2}\left(k\,x+c\,y-2^{2n-2}\,k\eta\,t\right)\right)\right),\quad n\in\mathbb{R}.
\end{aligned} \tag{2.19}$$

$$\begin{aligned}
\Psi_{11,12} &= \frac{2\,k\eta}{c(\delta+\lambda)+\gamma k}\left(1 \mp \frac{3}{\sin(kx+cy+k\eta\,t)\pm 1}\right),\\
\Phi_{11,12} &= \frac{2\,c\eta}{c(\delta+\lambda)+\gamma k}\left(1 \mp \frac{3}{\sin(kx+cy+k\eta\,t)\pm 1}\right).
\end{aligned} \tag{2.20}$$

$$\begin{aligned}
\Psi_{13} &= -\frac{\sigma_1}{2}\exp\left(-\frac{2\,k\left((\delta+\lambda)\,x-\gamma\,y+4k^2\,(\beta\gamma-\alpha(\delta+\lambda))\,t\right)}{\delta+\lambda}\right),\\
\Phi_{13} &= -\frac{\gamma\sigma_1}{2\,(\delta+\lambda)}\exp\left(-\frac{2\,k\left((\delta+\lambda)\,x-\gamma\,y+4k^2\,(\beta\gamma-\alpha(\delta+\lambda))\,t\right)}{\delta+\lambda}\right).
\end{aligned} \tag{2.21}$$

All of these solutions refer to types of wave structures predicted by the GBSS. They mainly refer to hyperbolic and trigonometric functions, including sech^2, csch^2, $\sec^2$, and $\csc^2$, each one characterizing localized solitons or periodic waveforms. However, the hyperbolic functions usually represent localized solitons that decay exponentially or quickly. While the trigonometric functions show periodic wave structures with periodic peaks or troughs, the constants and parameters control these solitons' speed, shape, and direction, traveling in the x- and y-directions over time. While Ψ_1 and

Ψ_2 demonstrate basic solitons with exponential decay in space (while also being strongly affected by boundary conditions), Ψ_3 and Ψ_4 show the general complexity of solitons, where they can already be multiple-peaked or even multi-dipped. However, solutions of the form Ψ_7, Ψ_8, and $\Psi_{11,12}$, which incorporate trigonometric functions, have a more oscillatory or periodic nature. These solutions are composed of waveforms with sharply formed and highly arcane peaks or oscillations across space; they lead to periodic activity rather than simply exponential decay. Due to combinations of constants with secant or cosecant functions, some solutions like Ψ_9 and Ψ_{10} produce solitons where noticeable peaks or dips are present in their center. These solutions can describe different wave behaviors, including localized solitons and periodic wave trains, and they consist of real physical representations due to the types of functions used (trigonometric/hyperbolic) in many of them.

For the next sections, the analysis will concern the properties and types of soliton solutions. This will be enhanced by an analysis of their dynamics, evolution, and importance within the framework of the non-linear system being investigated (1.1).

Figure 1 illustrates the exact solutions $\Psi_1(x,t)$ and $\Psi_3(x,t)$ for a set of values of n taken with step 0.5. Ψ_1 is symmetric and localized around the center at $x = 0$, whose amplitude increases drastically with n. This behavior reveals a soliton-like structure that is more localized for larger values of n. However, the right figure of Figure 1 shows Ψ_3, which has more localized peaks along with flat regions asymptotically. The solution will have a sign change, creating a dip (negative parts) and a peak (positive parts) around $x = 0$ and, for higher numbers, n, sharp changes. This indicates that parameter n controls the generalized shape and general amplitude of the solutions, which can be helpful in finding solutions to non-linear wave propagation that resembles waves such as solitons or localized energy regions.

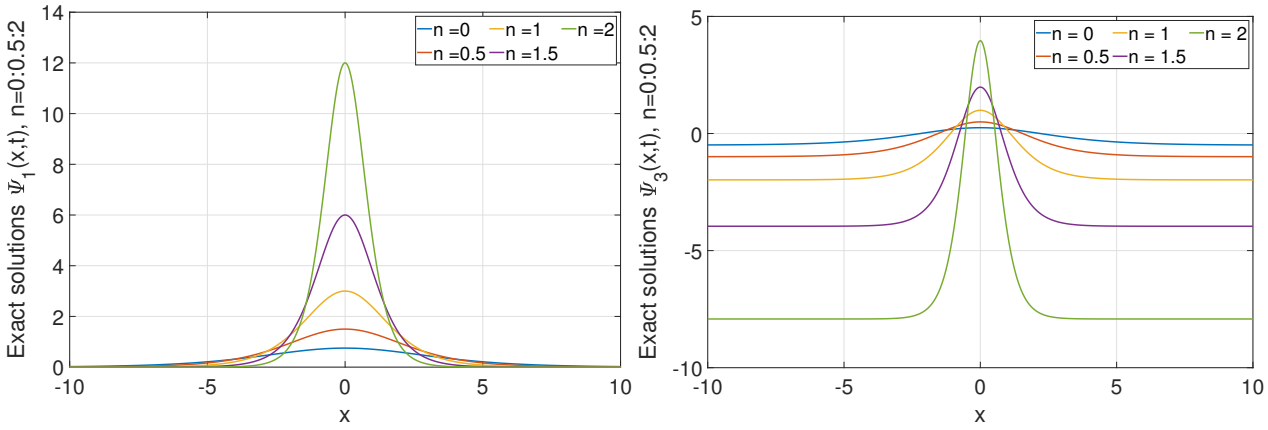

Figure 1. Exact solutions for $\Psi_1(x,t)$ and $\Psi_3(x,t)$ plotted for different values of n (ranging from 0 to 2 in steps of 0.5).

Figure 2 shows the impact of varying parameters α, β, γ, δ, λ on the behavior and dynamics of soliton at $t = 2$ for Ψ_1 and Ψ_3. The top and bottom left figures show the effects of α and β on $t = 2$, saying that when we increase both parameters for a fixed time moment, the soliton is more enhanced and local with a significant positive change in amplitude. The soliton for negative values becomes wider and smoother, with a lower peak, indicating that the energy is spread over a larger area. The positive values of α and β yield peaks higher and sharper, thus indicating energy more localized. The figures on the top and bottom right demonstrate the effects of γ, δ, and λ at $t = 2$, showing an identical behavior. Higher values of these parameters result in sharper solitons with increased amplitude, while lower or negative values lead to wider and less pronounced waves. In both cases, the soliton behavior shows that increasing the parameter values presses into a more compact high energy field configuration and decreasing them causes wave flattening and diluting.

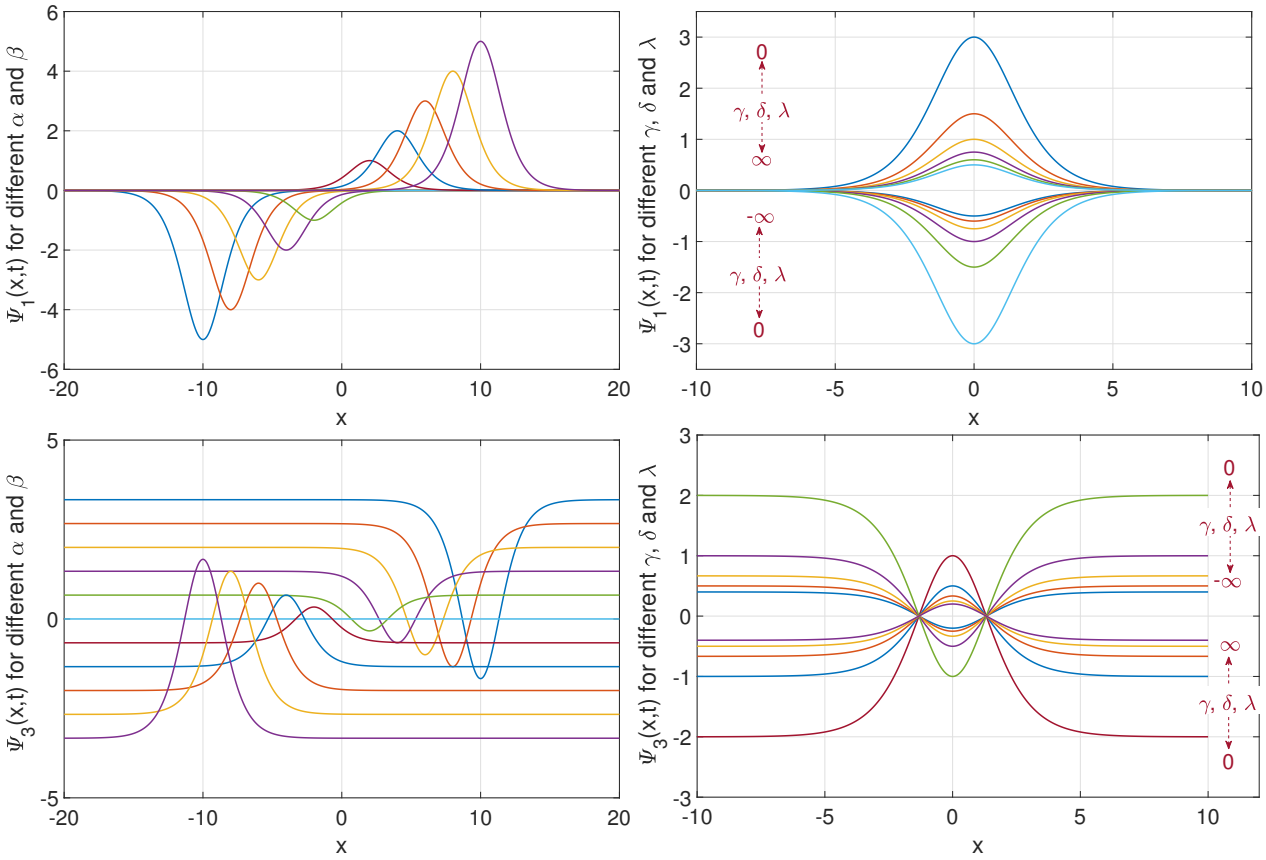

Figure 2. Plots of $\Psi_1(x, t)$ (top) and $\Psi_3(x, t)$ (bottom) for varying α, β, γ, δ, and λ.

Figure 3 shows the evolution of the soliton solutions $\Psi_1(x, y, t)$ and $\Psi_3(x, y, t)$ over increasing time, with five time-steps shown: $t = 0, 4, 8, 12, 16$, while the parameters used in these figures are as follows: $\alpha = 2.0$, $\beta = 0.5$, $\gamma = 0.6$, $\delta = -1.0$, $\lambda = 1.2$, $k = c = 1.0$, and $n = 1.0$. In figure (a), Ψ_1 moves in the positive x-direction in time while keeping the same shape and localization. In the figure (b), Ψ_3 instead evolves in the negative x-direction over time. This behavior illustrates the time and space evolution of the soliton solutions dynamic and directionality of Ψ_1 and Ψ_3 as they continue to evolve in opposite temporal and spatial directions.

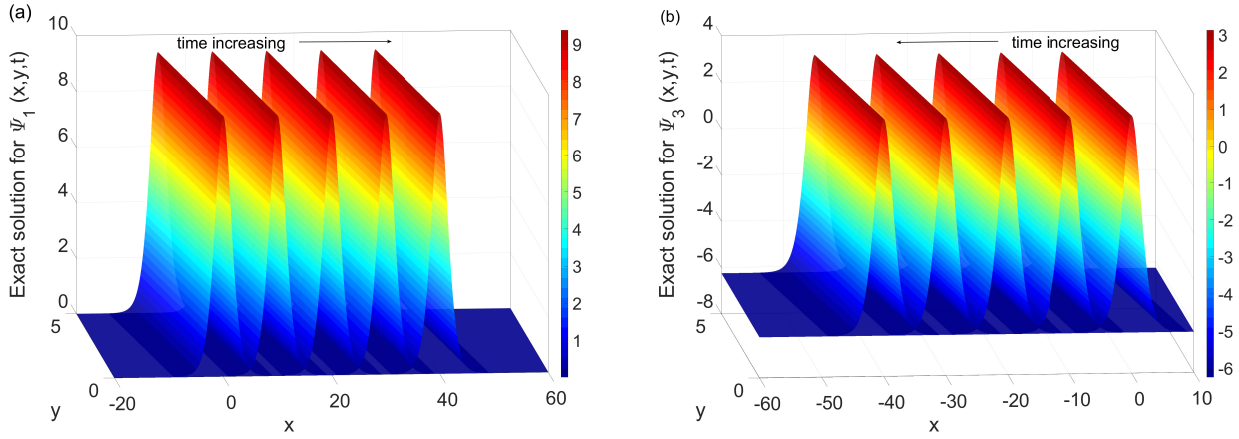

Figure 3. Two 3D figures of solitons are shown via the temporal development of exact solutions for $\Psi_1(x, y, t)$ and $\Psi_3(x, y, t)$ at times $(t = 0, 4, 8, 12, 16)$. The parameter values are taken by $\alpha = 2.0$, $\beta = 0.5$, $\gamma = 0.6$, $\delta = -1.0$, $\lambda = 1.2$, $k = c = 1.0$, and $n = 1.0$.

3. Numerical solutions of GBSS

This section discusses numerical solutions to the resulting ODE (2.8) using various numerical approaches. This approach aims to validate the accuracy of the analytical solutions. As a representative model, we selected one of the above analytic solutions, (2.11). The non-linear shooting and boundary value problem (BVP) methods, implemented at $t = 0$, utilize the value of ρ at the right endpoint of the domain $\zeta = 0$ while making an initial guess for ρ_ζ. The goal is to get the second boundary condition of ρ at the other endpoint. After getting the numerical results, we compare them with the analytical solution. The MATLAB solvers ODE15s and FSOLVE [39] are utilized to explore the numerical solution. To implement the BVP method, we discretize the resultant ODE (2.8) as follows:

$$\begin{aligned} &f(\rho) = 0, \\ &f(\rho_i) = -w\,\rho_i + \frac{k^2\,(k\,\alpha\, + c\,\beta\,)}{\Delta_\zeta^2}\,(\rho_{i+1} - 2\rho_i + \rho_{i-1}) + \frac{\frac{1}{2}\,(k\,\gamma\, + c\,\delta + c\,\lambda)}{2\Delta_\zeta}\left(\rho_{i+1}^2 - \rho_{i-1}^2\right). \end{aligned} \tag{3.1}$$

To apply the non-linear shooting method, the ODE (2.8) is discretized as follows:

$$\rho_{\zeta\zeta} = \frac{1}{k^2\,(k\,\alpha\, + c\,\beta\,)}\left(w\rho - \left(\frac{1}{2}\,(k\,\gamma\, + c\,\delta + c\,\lambda)\right)\rho^2\right). \tag{3.2}$$

Figure 4 compares the respective analytical solution to the numerical solution obtained by the shooting and the BVP methods. The numerical solutions are evaluated at $t = 0$, $y = 1.5$, and the spatial range $x \in [-55, 15]$. The analytical solution roughly matches both numerical solutions, including the narrow symmetric peak after $x = -1.55$. There is a comparison of methods studied and numerical problems solution efficiency. Results from the shooting or the BVP approaches provide a numerical solution, which will be used as the basis for the following numerical scheme. More specifically, these results will serve as initial conditions for the numerical scheme presented in the next section. This guarantees that the numerical scheme always begins with the correct and cohesive data, aiding in convergence for the controlling equations around the problem parameters and boundary conditions.

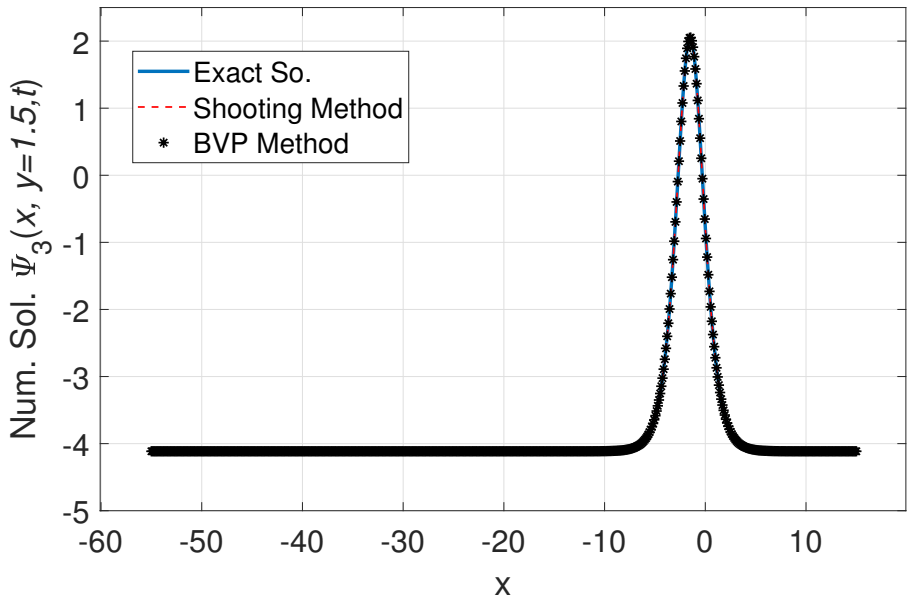

Figure 4. Evaluating the numerical solutions obtained from the shooting and boundary value problem approaches against the analytical solution (2.13) at $t = 0$, $y = 1.5$, and $x = -55 : 15$. The parameter values are taken as $\alpha = 0.6, \beta = 1.1, \gamma = -0.6, \delta = 1.3, \lambda = 0.3, k = c = 1.1$, and $n = 1$ with $M = 600$.

3.1. Numerical scheme

This section employs the finite-difference method to derive the numerical results of system (1.1) within the domain $[x_0, x_M] \times [y_0, y_N]$. In this context, x_0, y_0, x_M, and y_N define the bounds of the rectangular domain along the x- and y-axes, with T_f signifying a specific time. The domain is divided into $(M + 1) \times (N + 1)$ mesh points:

$$\begin{aligned} x_i &= x_0 + i\,h_x \qquad i = 0, 1, \ldots, M, \\ y_j &= y_0 + j\,h_y \qquad j = 0, 1, \ldots, N, \end{aligned}$$

where h_x and h_y denote the step sizes for the x and y domains, respectively. The system (1.1) is transformed into an ODE system by discretising the spatial derivatives while maintaining the continuity of the time derivative. Performing this results in

$$\begin{aligned} &\Psi_t|^k_{m,n} + \frac{\alpha}{2h_x^3}\left(\Psi^{k+1}_{m+2,n} - 2\Psi^{k+1}_{m+1,n} + 2\Psi^{k+1}_{m-1,n} - \Psi^{k+1}_{m-2,n}\right) \\ &\quad + \frac{\beta}{2h_x^2 h_y}\left(\Psi^{k+1}_{m+1,n+1} - \Psi^{k+1}_{m+1,n-1} - 2\left(\Psi^{k+1}_{m,n+1} - \Psi^{k+1}_{m,n-1}\right) + \Psi^{k+1}_{m-1,n+1} - \Psi^{k+1}_{m-1,n-1}\right) \\ &\quad + \frac{\gamma}{2h_x}\Psi^{k+1}_{m,n}\left(\Psi^{k+1}_{m+1,n} - \Psi^{k+1}_{m-1,n}\right) + \frac{\delta}{2h_x}\Psi^{k+1}_{m,n}\left(\Phi^{k+1}_{m+1,n} - \Phi^{k+1}_{m-1,n}\right) \\ &\quad + \frac{\lambda}{2h_x}\left(\Psi^{k+1}_{m+1,n} - \Psi^{k+1}_{m-1,n}\right)\Phi^{k+1}_{m,n} = 0 \\ &\frac{1}{2h_y}\left(\Psi^{k+1}_{m,n+1} - \Psi^{k+1}_{m,n-1}\right) = \frac{1}{2h_x}\left(\Phi^{k+1}_{m+1,n} - \Phi^{k+1}_{m-1,n}\right) \end{aligned} \tag{3.3}$$

subject to the boundary conditions:

$$\begin{aligned} \Psi_x(x_0, y, t) = \Psi_x(x_m, y, t) = 0, \qquad \forall y \in [y_0, y_m], \\ \Psi_y(x, y_0, t) = \Psi_y(x, y_m, t) = 0, \qquad \forall x \in [x_0, x_m], \end{aligned} \tag{3.4}$$

where $\alpha, \beta, \gamma, \delta, \lambda, k$, and c are user-defined parameters. Equation (3.4) allows for the use of fictitious points in the calculation of spatial derivatives at the boundaries of the domain. In the numerical results provided in this section, the parameter values are established as follows: $\alpha = 0.6, \beta = 1.1, \gamma = -0.6, \delta = 1.3, \lambda = 0.3, x_0 = -20, y = 0 \to 5, x = -55 \to 15$, and $t = 0 \to 20$.

We used MATLAB version R2023b on a PC equipped with an Intel® Core™ i7 processor operating at 3.40 GHz, 16 GB of RAM, and running Windows 11 to carry out our simulations. To solve implicit ODEs (3.3), the solver ODE15i uses the implicit, multi-step numerical method called the backward differentiation formulas (BDF). The technique has proven very effective in stiff systems and equations with complicated implicit conditions as it approximates derivatives with the previous time steps of the solution. Algorithms like Newton's iteration are used to solve non-linear systems resulting from the implicit formulation. The ODE15i solver is well-known for its accuracy and efficiency, especially with systems that are challenging for explicit methods. This is demonstrated by Figure 5.

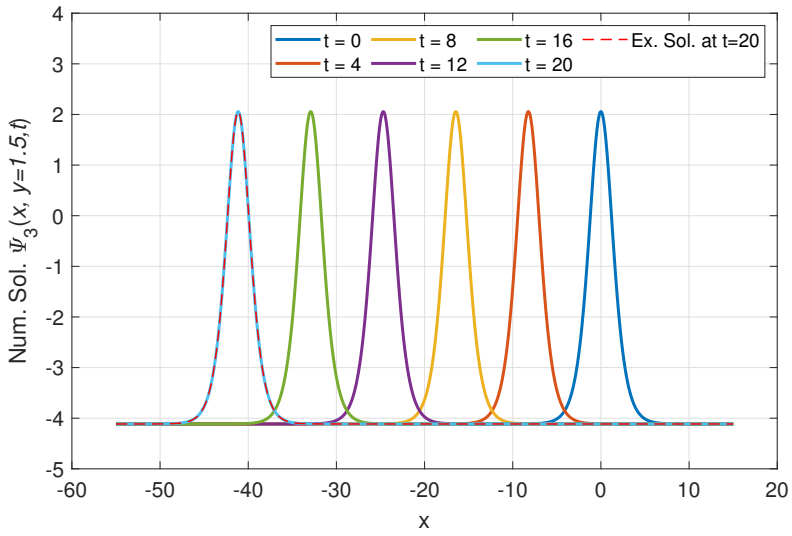

Figure 5. Numerical solution of $\Psi_1(x, y = 1.5, t)$ over space x for various time steps $t = 0, 4, 8, 12, 16$, and 20, illustrating the evolution of the solution and its convergence towards the exact solution at $t = 20$.

Figure 6 illustrates the comparison of the exact solution and the numerical solution of $\Psi_3(x, y = 1.5, t = 20)$ as the number of points varies. As can be seen, Figure 6 provides an appropriate agreement between numerical and exact solutions, which is evidence of the high reliability of numerical models. It also shows improved numerical precision as the spatial resolution is now finer.

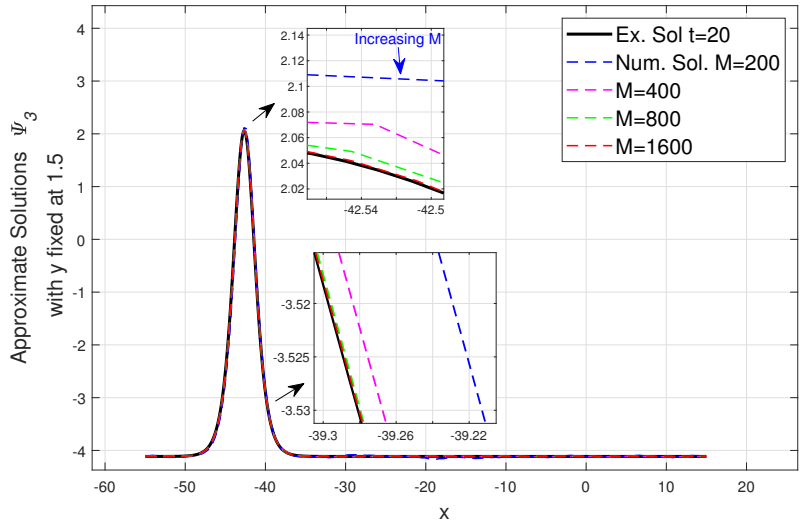

Figure 6. Comparison of approximation solutions Ψ_3 at $y = 1.5$ for different spatial grade for $t = 20$. Insets illustrate the convergence behavior as M grows.

Figure 7 offers a graphical illustration of how closely the numerical computations approximated the third wave function Ψ_3. The comparison enables us to appreciate the degree of effectiveness and correctness of the numerical method and highlights the inherent problems and quantifies the extent of stability of the solution within the specified domain. The following values were taken for the calculations: $\alpha = 0.6$, $\beta = 1.1$, $\gamma = -0.6$, $\delta = 1.3$, and $\lambda = 0.3$. Additionally, the spatio-temporal limits are $x \in [-55, 15]$, $y \in [0, 5]$, and $t \in [0, 20]$, respectively. Finally, in the respect to the resolution numerical parameters, a total of $M = 2300$ and $N = 150$ are set for the x- and y-directions, respectively, enabling for high precision to be maintained throughout the range set earlier on.

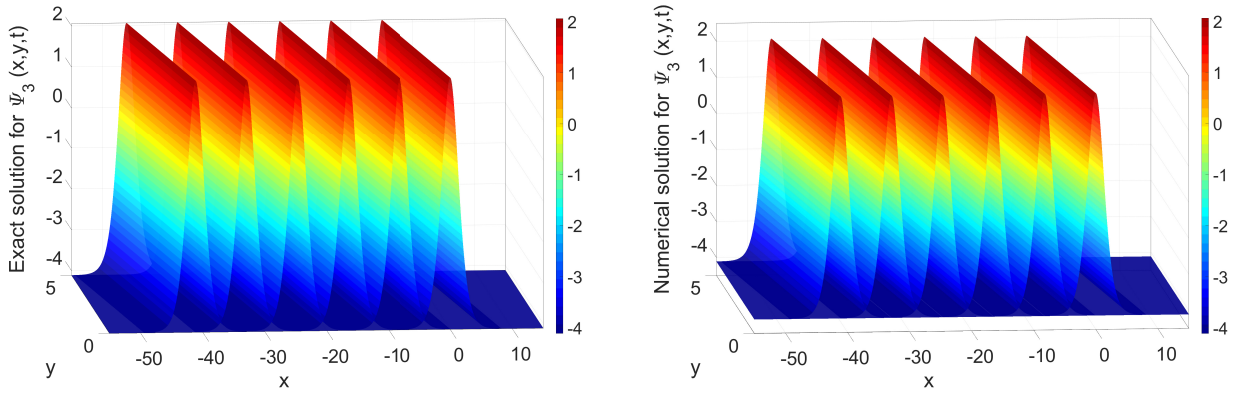

Figure 7. Comparison of exact and numerical solutions for Ψ_3, visualized across a two-dimensional plane.

3.2. Stability of the numerical scheme

Von Neumann analysis is applied to determine the stability of the scheme (3.3). Von Neumann analysis, sometimes referred to as Fourier analysis, is applied exclusively in the context of linear

systems. Therefore, we propose that the linear version is represented by

$$\Psi_t + \alpha\Psi_{xxx} + \beta\Psi_{yyy} + r_0\Psi_x + r_1\Psi_y + r_2\Psi_x = 0, \tag{3.5}$$

where $r_0 = \gamma\Psi$, $r_1 = \delta\Psi$, and $r_2 = \lambda\Phi$ are constant quantities defined as

$$r_0 = \max_{\substack{1\le m\le M\\ 1\le n\le N}} \left(\gamma\Psi_{m,n}^k\right), \quad r_1 = \max_{\substack{1\le m\le M\\ 1\le n\le N}} \left(\delta\Psi_{m,n}^k\right), \quad r_2 = \max_{\substack{1\le m\le M\\ 1\le n\le N}} \left(\lambda\Phi_{m,n}^k\right).$$

We assume a solution form:

$$\Psi_{m,n}^k = \exp\left(a\,k\,h_t \;+\; i\,b\,m\,h_x \;+\; i\,c\,n\,h_y\right). \tag{3.6}$$

As a result, we are able to write

$$\begin{aligned} \Psi_{m,n}^{k+1} &= \exp(a\,h_t)\,\Psi_{m,n}^k, \quad \Psi_{m\pm2,n}^k = \exp(\pm 2i\,b\,h_x)\,\Psi_{m,n}^k, \quad \Psi_{m,n\pm2}^k = \exp(\pm 2i\,c\,h_y)\,\Psi_{m,n}^k,\\ &\Psi_{m\pm1,n}^k = \exp(\pm i\,b\,h_x)\,\Psi_{m,n}^k, \quad \Psi_{m,n\pm1}^k = \exp(\pm i\,c\,h_y)\,\Psi_{m,n}^k. \end{aligned}$$

Substituting (3.6) into (3.5) and doing some operations yields

$$\begin{aligned} 1 = \exp(ah_t)\Bigg(1 - i\,h_t\Bigg(&\frac{\alpha\,(2\sin(bh_x) - \sin(2bh_x))}{h_x^3} + \frac{\beta\left(2\sin\left(ch_y\right) - \sin\left(2ch_y\right)\right)}{h_y^3}\\ &- \frac{r_1\sin\left(ch_y\right)}{h_y} - \frac{(r_0+r_2)\sin(bh_x)}{h_x}\Bigg)\Bigg). \end{aligned} \tag{3.7}$$

Hence,

$$\exp(ah_t) = \frac{1}{1 - F\,i}, \tag{3.8}$$

where

$$\begin{aligned} F = h_t\Bigg(&\frac{\alpha\,(2\sin(bh_x) - \sin(2bh_x))}{h_x^3} + \frac{\beta\left(2\sin\left(ch_y\right) - \sin\left(2ch_y\right)\right)}{h_y^3}\\ &- \frac{r_1\sin\left(ch_y\right)}{h_y} - \frac{(r_0+r_2)\sin(bh_x)}{h_x}\Bigg). \end{aligned}$$

Thus,

$$\left|\exp(ah_t)\right| = \frac{1}{\sqrt{1+F^2}} \le 1. \tag{3.9}$$

Equation (3.9) indicates the absence of growth, thus the stability condition of the von Neumann analysis is satisfied. As a result, the scheme is unconditionally stable.

3.3. Error analysis

To effectively evaluate the accuracy of numerical scheme (3.3), we perform a comprehensive investigation of the truncation error, $T(x, y, t)$, using Taylor series expansions. This method allows

a systematic analysis of the error's behavior and provides a basis for evaluating the scheme's accuracy under various circumstances. Suppose that the error is

$$e_{m,n}^{k+1} = \Psi_{m,n}^{k+1} - \Psi(x_m, y_n, t_{k+1}), \tag{3.10}$$

where $\Psi(x_m, y_n, t_{k+1})$ denotes the analytical solution, whereas $\Psi_{m,n}^{k+1}$ denotes the approximate numerical solution. Substituting (3.10) into (3.3) gives

$$\begin{aligned}\frac{e_{m,n}^{k+1} - e_{m,n}^{k}}{h_t} = T_{m,n}^{k+1} - \Bigg(&\frac{\alpha}{2h_x^3}\left(e_{m+2,n}^{k+1} - 2e_{m+1,n}^{k+1} + 2e_{m-1,n}^{k+1} - e_{m-2,n}^{k+1}\right) \\ &+ \frac{\beta}{2h_y^3}\left(e_{m,n+2}^{k+1} - 2e_{m,n+1}^{k+1} + 2e_{m,n+1}^{k+1} + e_{m,n+2}^{k+1}\right) \\ &+ \frac{(r_0 + r_2)}{2h_x}\left(e_{m+1,n}^{k+1} - e_{m-1,n}^{k+1}\right) + \frac{r_1}{2h_x}\left(\Psi_{m,n-1}^{k+1} - \Psi_{m,n-1}^{k+1}\right)\Bigg).\end{aligned} \tag{3.11}$$

We are given that

$$\begin{aligned}T_{m,n}^{k+1} = &\frac{\alpha}{2h_x^3}\left(\Psi(x_{m+2}, y_n, t_{k+1}) - 2\Psi(x_{m+1}, y_n, t_{k+1}) + 2\Psi(x_{m-1}, y_n, t_{k+1}) - \Psi(x_{m-2}, y_n, t_{k+1})\right) \\ &+ \frac{\beta}{2h_y^3}\left(\Psi(x_m, y_{n+2}, t_{k+1}) - 2\Psi(x_m, y_{n+1}, t_{k+1}) + 2\Psi(x_m, y_{n-1}, t_{k+1}) - \Psi(x_m, y_{n-2}, t_{k+1})\right) \\ &+ \frac{(r_0 + r_2)}{2h_x}\left(\Psi(x_{m+1}, y_n, t_{k+1}) - \Psi(x_{m-1}, y_n, t_{k+1})\right) \\ &+ \frac{r_1}{2h_x}\left(\Psi(x_m, y_{n+1}, t_{k+1}) - \Psi(x_m, y_{n-1}, t_{k+1})\right).\end{aligned}$$

Thus

$$\begin{aligned}T_{m,n}^{k+1} \leq &\frac{h_t}{2}\frac{\partial^2 \Psi(x_m, y_n, \xi_{k+1})}{\partial t^2} - \frac{h_x^2}{4}\frac{\partial^5 \Psi(\zeta_m, y_n, t_{k+1})}{\partial x^5} - \frac{h_y^2}{4}\frac{\partial^5 \Psi(x_m, \eta_n, t_{k+1})}{\partial y^5} \\ &- \frac{h_y^2}{6}\frac{\partial^3 \Psi(x_m, \eta_n, t_{k+1})}{\partial y^3} - \frac{h_x^2}{6}\frac{\partial^3 \Psi(\zeta_m, y_n, t_{k+1})}{\partial x^3}.\end{aligned}$$

Consequently, the truncation error of the numerical scheme is

$$T_{m,n}^{k+1} = O(h_t, h_x^2, h_y^2).$$

Table 2 and Figure 8 demonstrate the relationship between numerical accuracy and computational effort across varying (h_x) at $t = 20$. Table 2 illustrates the relative error in the L_2 norm with corresponding CPU time, which indicates that fine (h_x) will lead to increased accuracy, although with more significant computational needs. This trade-off points out the computational expense that is linked to achieving reduced errors. Figure 8 displays the convergence of the numerical method, which exhibits a slope of roughly 1.9, which indicates its second-order accuracy. The analysis emphasises a specific variable ($y = 0.5$) and computational domain ($x \in [-55, 15]$), which provides an accurate measurement of the method's performance. This finding highlights the necessary balance between accuracy and efficiency in computational simulations.

Table 2. Relative error in L_2 norm and CPU time for various grid resolutions (h_x) at $t = 20$. The data shows the computational accuracy-time trade-off.

Δ_x	Relative Error	CPU
0.6000	1.030×10^{0}	1.140×10^{-1} s
0.3000	4.870×10^{-2}	4.310×10^{-1} s
0.1500	2.600×10^{-3}	2.649×10^{0} s
0.0750	3.145×10^{-4}	3.012×10^{1} s
0.0375	2.810×10^{-5}	2.795×10^{2} s
0.0187	2.310×10^{-5}	4.0230×10^{3} s

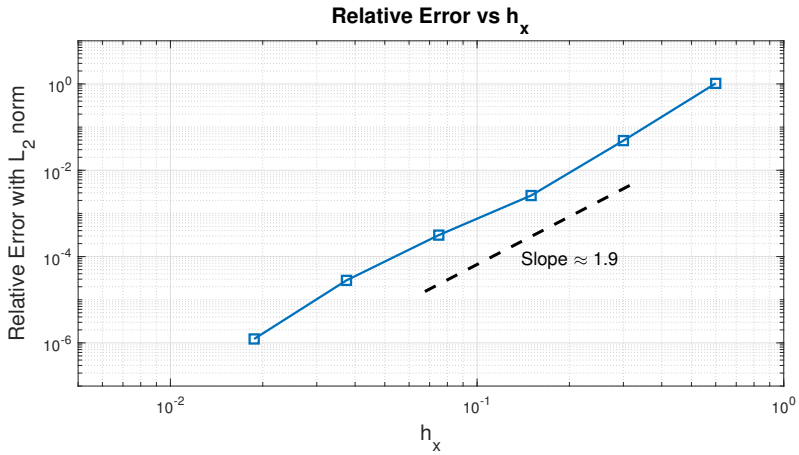

Figure 8. Log-log plot of the relative error (L_2 norm) against grid spacing (h_x), which shows numerical convergence with a slope of roughly 1.9, which signifies the second-order accuracy of the numerical method (see Table 2). In this instance, we selected a specific value for the variable, $y = 0.5$, at $t = 20$ and $x \in [-55, 15]$.

4. Conclusions

We addressed numerical and analytical investigations for the (2+1)-dimensional GBSS model. In this paper, we applied more improved analytical and computational approaches, such as the modified F-expansion, and were able to extract exact solutions. These solutions exhibit the remarkable property of solitons, which is the ability to keep their shape and remain stable over particularly large distances for broad periods of time, which plays a key role in cases of non-linear wave dynamics. Theoretical models were validated by the use of robust numerical algorithms such as finite difference and boundary-value problem approaches. The results that were predicted during the numerical simulations corresponded to predictions made by the theories that were posed, and our analytical approaches were also proved correct. Moreover, the results suggest potential practical applications of these solutions as solitons. Consider the case where solitons can travel through fibers, neither changing shape nor dissipating energy, in optical communication systems. If so, they could increase channel capacity and lower bit-error rates, enabling data to travel more smoothly. Similarly, the insights gained may be helpful in fluid mechanics and plasma physics, where managing non-linear wave propagation is crucial. The

contribution of analytical and numerical solutions not only contributes to a deeper understanding of the complex processes describing the GBSS but also shows the efficiency of our approaches in modeling complicated non-linear phenomena. In general, this study serves as a theoretical foundation for further scientific advancements and offers practical means for technological advancements in spheres that require extensive insights into non-linear wave behaviors.

Author contributions

Amer Ahmed: Conceptualization, methodology, formal analysis, validation, and writing original draft; Abdulghani R. Alharbi (arharbi@taibahu.edu.sa): Conceptualisation, investigation, data curation, and visualization; Ishak Hashim (ishak_h@ukm.edu): Supervision and writing review and editing. All authors have read and approved the final version of the manuscript for publication.

Use of Generative-AI tools declaration

The authors declare that they have not used artificial intelligence (AI) tools to create this article.

Acknowledgments

The author, Amer Ahmed, is grateful to Taibah University for its generous support in the form of a fully paid scholarship, which significantly helped in successfully completing this work.

Conflict of interest

The authors declare no conflicts of interest.

References

1. A. Seadawy, I. Mujahid, Optical soliton solutions for non-linear complex Ginzburg–Landau dynamical equation with laws of nonlinearity Kerr law media, *Int. J. Mod. Phys. B,* **34** (2020), 2050179. https://doi.org/10.1142/S0217979220501799
2. A. Wazwaz, Gaussian solitary waves for the logarithmic Boussinesq equation and the logarithmic regularised Boussinesq equation, *Ocean Eng.,* **94** (2015), 111–115. https://doi.org/10.1016/j.oceaneng.2014.11.024
3. B. Li, Y. Ma, T. Yang, Stable optical soliton in the ring-cavity fiber system with carbon nanotube as saturable absorber, *Superlattice. Microst.,* **113** (2018), 366–372. https://doi.org/10.1016/j.spmi.2017.11.016
4. J. Yang, Y. Gao, C. Su, D Zuo, Y. Feng, Solitons and quasi-periodic behaviors in an inhomogeneous optical fiber, *Commun. Nonlinear Sci.,* **42** (2017), 477–490. https://doi.org/10.1016/j.cnsns.2016.05.013
5. H. Ismael, T. Sulaiman, H. Nabi, W. Mahmoud, M. Osman, Geometrical patterns of time variable Kadomtsev–Petviashvili (I) equation that models dynamics of waves in thin films with high surface tension, *Nonlinear Dyn.,* **111** (2023), 9457–9466. https://doi.org/10.1007/s11071-023-08319-8

6. M. Zhang, Y. Ma, B. Li, Novel loop-like solitons for the generalized Vakhnenko equation, *Chinese Phys. B,* **22** (2013), 030511. https://dx.doi.org/10.1088/1674-1056/22/3/030511
7. A. R. Seadawy, Stability analysis for Zakharov–Kuznetsov equation of weakly non-linear ion-acoustic waves in a plasma, *Comput. Math. Appl.,* **67** (2014), 172–180. https://doi.org/10.1016/j.camwa.2013.11.001
8. Y. Ma, B. Li, The wrinkle-like N-solitons for the thermophoretic motion equation through graphene sheets, *Physica A,* **494** (2018), 169–174. https://doi.org/10.1016/j.physa.2017.12.014
9. B. Ren, P. Chu, Dynamics of D'Alembert wave and soliton molecule for a (2+1)-dimensional generalized breaking soliton equation, *Chinese J. Phys.,* **74** (2021), 296–301. https://doi.org/10.1016/j.cjph.2021.07.025
10. B. Ren, J. Lin, Z. Lou, Consistent Riccati expansion and rational solutions of the Drinfel'd–Sokolov–Wilson equation, *Appl. Math. Lett.,* **105** (2020), 106326. https://doi.org/10.1016/j.aml.2020.106326
11. M. Remoissenet, *Basic concepts and the discovery of solitons. Waves Called Solitons: Concepts and Experiments*, Heidelberg: Springer Berlin Heidelberg, 1999. https://doi.org/10.1007/978-3-662-03790-4_1
12. C. Becker, S. Stellmer, P. Soltan-Panahi, S. Dörscher, M. Baumert, E. Richter, et al., Oscillations and interactions of dark and dark–bright solitons in Bose–Einstein condensates, *Nat. Phys.,* **4** (2008), 496–501. https://doi.org/10.1038/nphys962
13. A. Slunyaev, Persistence of hydrodynamic envelope solitons: Detection and rogue wave occurrence, *Phys. Fluids,* **33** (2021), 036606. https://doi.org/10.1063/5.0042232
14. G. Dematteis, T. Grafke, E. Eijnden, Rogue waves and large deviations in deep sea, *P. Natl. Acad. Sci.,* **115** (2018), 855–860. https://www.pnas.org/doi/abs/10.1073/pnas.1710670115
15. A. Alharbi, Traveling-wave and numerical solutions to non-linear evolution equations via modern computational techniques, *AIMS Math.,* **9** (2024), 1323–1345. https://doi.org/10.3934/math.2024065
16. S. Residori, M. Onorato, U. Bortolozzo, F. Arecchi, Rogue waves: A unique approach to multidisciplinary physics, *Contemp. Phys.,* **58** (2017), 53-–69. https://doi.org/10.1080/00107514.2016.1243351
17. A. Demircan, S. Amiranashvili, C. Brée, C. Mahnke, F. Mitschke, G. Steinmeyer, Rogue events in the group velocity horizon, *Sci. Rep.,* **2** (2012), 850. https://doi.org/10.1038/srep00850
18. G. Xu, Integrability of a (2+1)-dimensional generalized breaking soliton equation, *Appl. Math. Lett.,* **50** (2015), 16–22. https://doi.org/10.1016/j.aml.2015.05.015
19. L. Ling, L. Zhao, B. Guo, Darboux transformation and classification of solution for mixed coupled non-linear Schrödinger equations, *Commun. Nonlinear Sci.,* **32** (2016), 285–304. https://doi.org/10.1016/j.cnsns.2015.08.023
20. S. Jia, Y. Gao, C. Zhao, Z. L. Feng, Solitons, breathers and rogue waves for a sixth-order variable-coefficient non-linear Schrödinger equation in an ocean or optical fiber, *Eur. Phys. J. Plus,* **132** (2017), 34. https://doi.org/10.1140/epjp/i2017-11318-y

21. R. Hirota, Exact solution of the modified Korteweg-de Vries equation for multiple collisions of solitons, *J. Phys. Soc. Japan,* **33** (1972), 1456–1458. https://doi.org/10.1143/JPSJ.33.1456

22. B. Ghanbari, K. Nisar, Determining new soliton solutions for a generalized non-linear evolution equation using an effective analytical method, *Alex. Eng. J.,* **59** (2020), 3171–3179. https://doi.org/10.1016/j.aej.2020.07.032

23. A. Alharbi, Numerical solutions to two-dimensional fourth order parabolic thin film equations using the Parabolic Monge-Ampere method, *AIMS Math.,* **8** (2023), 16463–16478. https://doi.org/10.3934/math.2023841

24. A. Alharbi, Traveling-wave and numerical solutions to a Novikov-Veselov system via the modified mathematical methods, *AIMS Math.,* **8** (2023), 1230–1250. https://doi.org/10.3934/math.2023062

25. M. Iqbal, A. Seadawy, S. Althobaiti, Mixed soliton solutions for the (2+1)-dimensional generalized breaking soliton system via new analytical mathematical method, *Results Phys.,* **32** (2022), 105030. https://doi.org/10.1016/j.rinp.2021.105030

26. M. Jawad, A. Ja'afar, Soliton solutions for nonlinear systems (2+1)-dimensional equations, *IOSR J. Math.,* **1** (2012), 27–34. http://dx.doi.org/10.9790/5728-0162734

27. W. Hereman, M. Takaoka, Solitary wave solutions of non-linear evolution and wave equations using a direct method and MACSYMA, *J. Phys. A-Math. Gen.,* **23** (1990), 4805. https://dx.doi.org/10.1088/0305-4470/23/21/021

28. T. Alharbi, A. Alharbi, Traveling-wave and numerical investigations to non-linear equations via modern computational techniques, *AIMS Math.,* **9** (2024), 12188–12210. https://doi.org/10.3934/math.2024595

29. T. Alharbi, A. Alharbi, A study of traveling wave structures and numerical investigations into the coupled nonlinear schrödinger equation using advanced mathematical techniques, *Mathematics,* **11** (2023), 4597. https://doi.org/10.3390/math11224597

30. M. Ahmed, A. Zaghrout, H. Ahmed, Construction of solitons and other solutions for NLSE with Kudryashov's generalized non-linear refractive index, *Alex. Eng. J.,* **64** (2023), 391–397. https://doi.org/10.1016/j.aej.2022.09.015

31. I. Samir, E. Salah, E. A. El-Dahab, H. M. Ahmed, M. Ammar, W. Alexan, et al., Unraveling solitons dynamics in system of dispersive NLSE with Kudryashov's law of nonlinearity using improved modified extended tanh function method, *Alex. Eng. J.,* **91** (2024), 419–428. https://doi.org/10.1016/j.aej.2024.02.020

32. R. Attia, H. Qazi, A. Kamran, A. Jamshad, Z. Aniqa, Soliton solutions of nonlinear evolution equations by basic (G'/G)-expansion method, *Math. Model. Eng. Probl.,* **7** (2020), 242—250. http://dx.doi.org/10.18280/mmep.070210

33. F. Calogero, A. Degasperis, Non-linear evolution equations solvable by the inverse spectral transform.—I, *Nuovo Cimento B,* **32** (1976), 201–242. https://doi.org/10.1007/BF02727634

34. A. Wazwaz, A new integrable (2+1)-dimensional generalized breaking soliton equation: N-soliton solutions and traveling wave solutions, *Commun. Theor. Phys.,* **66** (2016), 385. https://dx.doi.org/10.1088/0253-6102/66/4/385

35. Y. Ma, B. Li, Interactions between soliton and rogue wave for a (2+1)-dimensional generalized breaking soliton system: Hidden rogue wave and hidden soliton, *Comput. Math. Appl.,* **78** (2019), 827–839. https://doi.org/10.1016/j.camwa.2019.03.002

36. T. Taklo, W. Choi, Group resonant interactions between surface and internal gravity waves in a two-layer system, *J. Fluid Mech.,* **892** (2020), A14. https://doi.org/10.1017/jfm.2020.180

37. V. Kruglov, J. Harvey, Solitary waves in optical fibers governed by higher-order dispersion, *Phys. Rev. A,* **98** (2018), 063811. https://link.aps.org/doi/10.1103/PhysRevA.98.063811

38. M. Abdou, The extended F-expansion method and its application for a class of non-linear evolution equations, *Chaos Soliton. Fract.,* **31** (2007), 95–104. https://doi.org/10.1016/j.chaos.2005.09.030

39. L. Shampine, M. Reichelt, The MATLAB ODE suite, *SIAM J. Sci. Comput.,* **18** (1997), 1–22. https://doi.org/10.1137/S1064827594276424

AIMS Press